Electrochemistry Communications 28 (2013) 40–43

Contents lists available at SciVerse ScienceDirect

Electrochemistry Communications

journal homepage: www.elsevier.com/locate/elecom

Interdispersed silicon–carbon nanocomposites and their application as anode materials for lithium-ion batteries

Zichao Yang [a], Juchen Guo [a], Shaomao Xu [a], Yingchao Yu [b], Héctor D. Abruña [b], Lynden A. Archer [a,*]

[a] School of Chemical and Biomolecular Engineering, Cornell University, Ithaca, NY 14853, USA
[b] Chemistry and Chemical Biology, Cornell University, Ithaca, NY 14853, USA

ARTICLE INFO

Article history:
Received 7 November 2012
Received in revised form 27 November 2012
Accepted 27 November 2012
Available online 2 December 2012

Keywords:
Silicon anodes
Silicon–carbon nanocomposites
Lithium ion battery

ABSTRACT

As an anode material for lithium-ion batteries (LIBs), silicon offers among the highest theoretical storage capacity, but is known to suffer from large structural changes and capacity fading during electrochemical cycling. Nanocomposites of silicon with carbon provide a potential material platform for resolving this problem. We report a spray-pyrolysis approach for synthesizing amorphous silicon–carbon nanocomposites from organic silane precursors. Elemental mapping shows that the amorphous silicon is uniformly dispersed in the carbon matrix. When evaluated as anode materials in LIBs, the materials exhibit highly, stable performance and excellent Coulombic efficiency for more than 150 charge discharge cycles at a charging rate of 1 A/g. Post-mortem analysis indicates that the structure of the Si–C composite is retained after extended electrochemical cycling, confirming the hypothesis that better mechanical buffering is obtained when amorphous Si is embedded in a carbon matrix.

1. Introduction

Currently used graphite anodes for lithium ion batteries (LIBs) provide a maximum storage capacity of 372 mAh/g. With a theoretical capacity of 4200 mAh/g and a low potential relative to Li/Li^+, silicon offers the potential for LIBs with more than ten-fold improvement in anode storage capacity. Development of such anodes has been hampered by the so-called pulverization problem [1], wherein large cyclic volume changes produced by repeated alloying/delloying reactions during electrochemical cycling of the battery induce fatigue failure of the active materials. This results in mechanical breakdown of the active Si particles, continuous reaction with the electrolyte to form new SEI film with each cycle, and gradual deterioration of electrical contact between the particles and conductive additives.

Many methods have been proposed to mitigate pulverization in Si, mainly through nanoscale design and creation of composites [1,2]. Lower dimensional Si nanostructures, such as thin films [3,4] nanowires,[5] nanotubes [6,7], nanoparticles [8] and mesoporous silicon [9] have proven particularly attractive because they allow enhanced strain relaxation, which should lead to improved structure retention. In practice, none of these approaches live up to their promise in providing stable battery cycling. Composites containing Si embedded in an inactive matrix (e.g. carbon) [10–12] or created by depositing Si on a carbon substrate [13,14] provide alternate approaches for buffering the strain produced during electrochemical cycling. For the embedding approach, a uniform distribution of Si particles is desirable to accommodate isotropic volume expansion. The most commonly practiced examples of this methodology all make use of crystalline silicon nanoparticles. The plane-strain form of the Griffith–Irwin relation [15], $\sigma_{fracture} = K_{IC}/(\pi c)^{1/2}$, indicates that the fracture strength $\sigma_{fracture}$ of an isotropic material is set by the material's fracture toughness $G_{IC} = (1-\nu^2)K^2_{IC}/E$, elastic modulus E, Poisson ratio ν, and typical flaw length c. Because amorphous particles are characterized by small grain sizes, their fracture strength is generally higher than crystalline ones. An amorphous particle also experiences isotropic stresses during volumetric change. Implying that a LIB anode based on amorphous Si uniformly embedded in a buffering host material such as carbon might be ideal for reducing stress fracture during alloying/dealloying reactions.

2. Materials and methods

Silicon–carbon nanocomposite powders comprised of amorphous silicon uniformly embedded in carbon were synthesized using a spray pyrolysis methodology [16]. In a typical synthesis, 3 ml of dimethyldivinylsilane (Gelest, Inc.) is mixed with 5 ml hexane (Aldrich) and the solution loaded into a 20-ml syringe, and atomized with argon stream in a collision-type nebulizer before entering a tubular furnace at 900 °C. The nominal residence time in the heated region is ~1 s. Thermal decomposition of the

* Corresponding author. Tel.: +1 607 255 4420; fax: +1 607 255 9166.
E-mail address: laa25@cornell.edu (L.A. Archer).

1388-2481/$ – see front matter
http://dx.doi.org/10.1016/j.elecom.2012.11.032

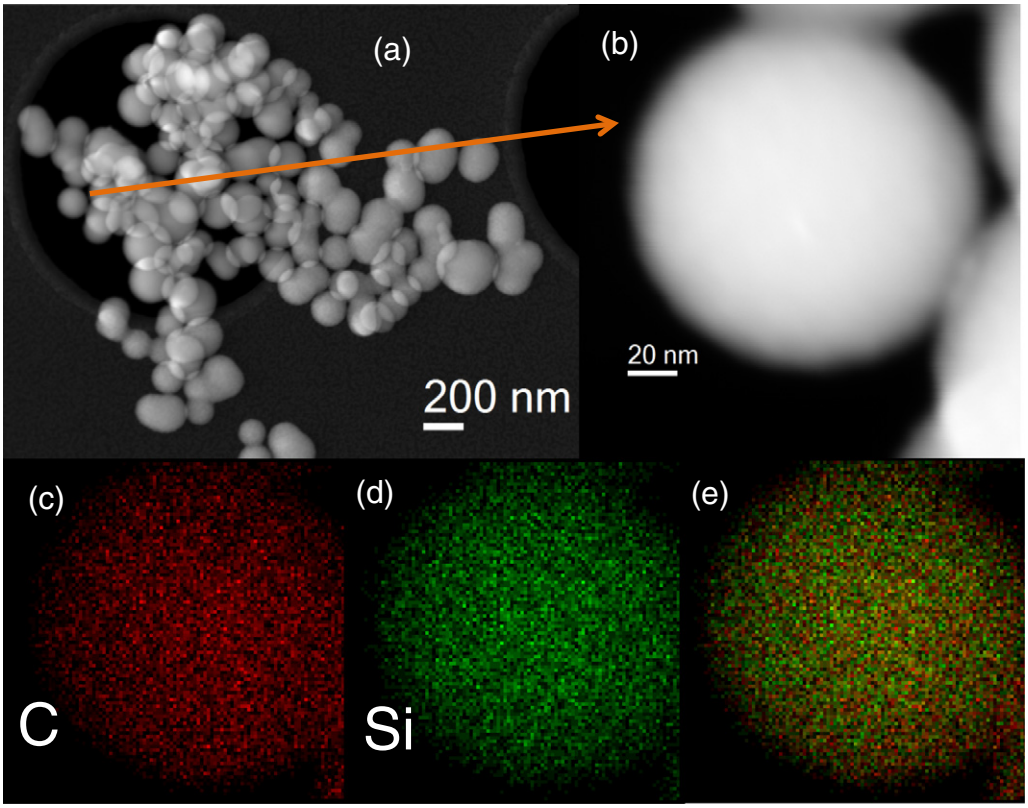

Fig. 1. High angle annular dark field (HAADF) scanning transmission electron microscopy (STEM) images of (a) the overview and (b) a representative nanoparticle, along with its energy dispersive X-ray (EDX) mapping of (c) carbon (d) silicon (e) composite of both elements. Both C and Si are homogenously distributed in the nanoparticle.

organic silane yields amorphous silicon and carbon. The final product Si–C nanocomposite particles are collected on a 0.4 μm (pore size) DTTP Millipore filter.

The Si–C nanocomposites were characterized using X-ray diffraction (Scintag Theta–Theta PAD-X X-ray Diffractometer (Cu Kα, λ = 1.5406 Å), TEM analysis (FEI Tecnai G2 T12 Spirit TEM (120 kV)), EDX elemental mapping (FEI Tecnai F20 TEM (200 kV)) and thermogravimetric analysis (TA Instruments Q5000 IR. Electrochemical properties of the materials were characterized at room temperature in 2032 coin-type cells using a Neware CT-3008 cycler and a CH Instruments CHI600D potentiostat. A working electrode comprised of 80 wt.% Si–C, 10 wt.% of carbon black (Super-P TIMCAL) and 10 wt.% PVDF was used. Copper foil (0.001 in., Alfa Aesar) was used as the current collector. Lithium foil (0.03 in., Alfa Aesar) was used as the counter and reference electrode. A 1 M solution of $LiPF_6$ in a 50/50 wt.% mixture of ethylene carbonate and diethylcarbonate was used as the electrolyte and Celgard 2500 polypropylene membranes as the separator.

3. Results and discussion

Silicon–carbon nanocomposite powders were synthesized using a spray pyrolysis method in which an organic silane is pyrolysed to form both silicon and carbon. By maintaining a short residence time (~1 s), the silicon is formed as amorphous nanoparticles in the carbon matrix. The weight fraction of Si is estimated to be 40% from TGA. Spray pyrolysis of citric acid has been used previously to create Si–C composites by coating amorphous carbon on preformed Si nanoparticles [17]; a homogeneous dispersion of Si in carbon is not possible with this approach. The present method eliminates the need for separate creation of silicon and carbon by using organic silane precursors for both the C and Si components. Importantly, it yields uniformly sized particles (Fig. 1) in which the carbon and Si are well distributed. A final advantage of the method over a previously reported silane pyrolysis scheme [18] is that it yields nanocomposites with greater Si content.

The distribution of silicon and carbon in the nanocomposites was characterized using EDX elemental analysis. STEM images of the Si–C particles are shown in Fig. 1(a) and (b). Fig. 1(c) and (d) shows elemental maps for C and Si and for all elements (e). It is apparent that Si is uniformly distributed in carbon throughout the particle. This is confirmed by line scan EDX spectra of the particles (Fig. 2(b)–(d)). The resolution of Fig. 2(b) is approximately 2.5 nm (as more clearly shown in Fig. 2(c)), which leads us to conclude that silicon and carbon are interdispersed at least down to the scale of 2–3 nm. XRD analysis presented in Fig. 2(e) shows broad features consistent with a partially graphitic carbon, but shows none of the characteristics for crystalline Si. This means that the Si phase is, as desired, completely amorphous.

Electrochemical properties of the Si–C nanocomposite particles were studied using cyclic voltammetry and galvanostatic cycling. Fig. 3(a) reports the charge capacity and Coulombic efficiency at a fixed rate of 1 A/g. The capacity results are all based on the active material mass in the anode and show that the material exhibits stable electrochemical cycling over 150 cycles, with excellent Coulombic efficiency. Fig. 3(b) nicely shows that these features are preserved at a range of charging rates: from 400 mA/g, 1 A/g, 2 A/g and 5 A/g.

To assess our hypothesis that the mechanical buffering effect of the carbon host is responsible for the improved electrochemical properties of the Si–C nanocomposites, post-mortem TEM and elemental analysis studies were performed. Fig. 4(a) and (b) shows typical images

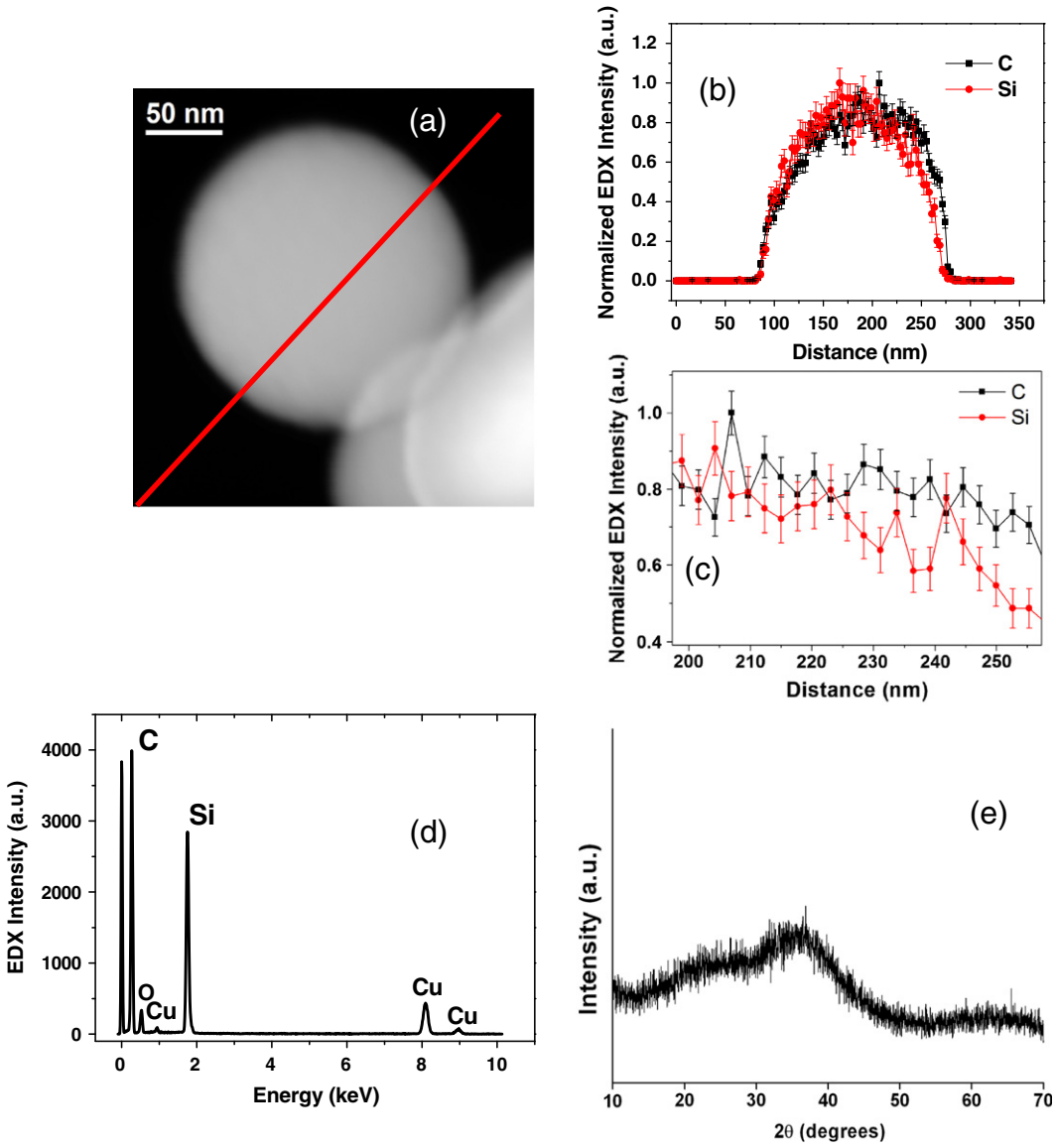

Fig. 2. (a) HAADF-STEM of a Si–C nanoparticle, along with (b) normalized EDX line profile, with error bars calculated from the Poisson noise and (c) the part of (b) between 200 and 250 nm zoomed in. (d) EDX spectrum acquired along the line profile and (e) XRD powder diffraction analysis of the Si–C nanocomposites.

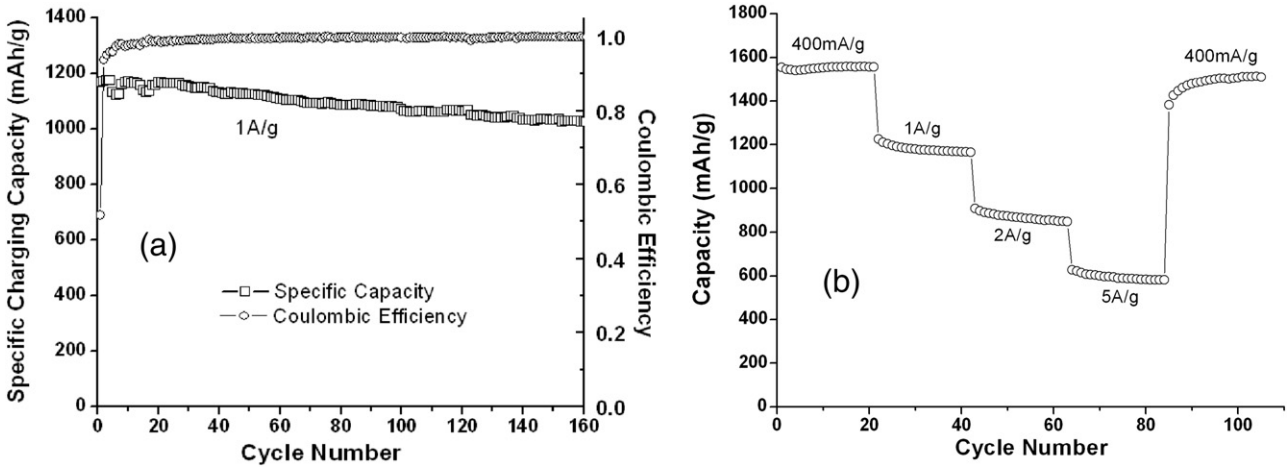

Fig. 3. Cycling performance of the Si–C composite (a) at 1 A/g and (b) at varied charging rates.

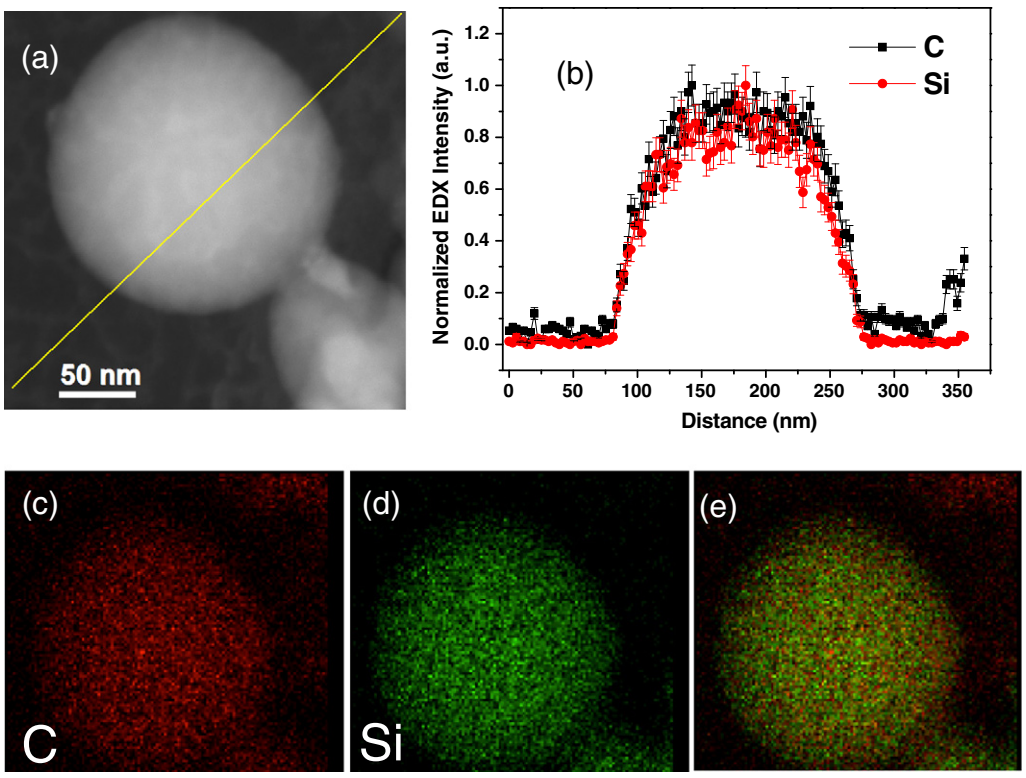

Fig. 4. Structure analysis after electrochemical cycling. HAADF-STEM images of a typical nanoparticle recovered from the Si–C anode. (b) Normalized EDX line-scan mapping of C and Si in particles after electrochemical cycling. EDX elemental maps for carbon (c), silicon (d), and a composite of both elements (e).

of the Si–C nanocomposite after 150 cycles, which show that the particles retain their shape, size and texture after repeated electrochemical cycling. The elemental maps (Fig. 4b–d) again show that the distribution of Si and C in the composite particles remains uniform. These results verify that the interdispersed amorphous silicon–carbon configuration has good structural stability and is not affected by the lithiation/delithiation process, a feature which mitigates pulverization and helps maintain stable cycling performance of silicon anodes.

4. Conclusions

In conclusion, we report a method for synthesizing interdispersed silicon–carbon nanocomposites based on spray pyrolysis. The presence of silicon in an amorphous form uniformly distributed throughout the carbon matrix is shown to help prevent pulverization and to improve cycling stability of Si-based LIB anodes. The *in situ* synthesis approach obviates the separate steps of silicon particle synthesis and carbon matrix creation, which is beneficial for scale-up processes for commercial scale production of the nanocomposites.

Acknowledgment

This material is based on work supported as part of the Energy Materials Center at Cornell, an Energy Frontier Research Center funded by the U.S. Department of Energy, Office of Science, Office of Basic Energy Sciences under Award Number DE-SC0001086. Y. Yu acknowledges the fellowship from ACS Division of Analytical Chemistry and support from Eastman Chemical Co. This work made use of the electron microscopy facility at the Cornell Center for Materials Research (CCMR), an NSF supported MRSEC through Grant DMR-1120296.

References

[1] J.R. Szczech, S. Jin, Energy & Environmental Science 4 (2011) 56.
[2] H.K. Liu, Z.P. Guo, J.Z. Wang, K. Konstantinov, Journal of Materials Chemistry 20 (2010) 10055.
[3] J.B. Bates, N.J. Dudney, B. Neudecker, A. Ueda, C.D. Evans, Solid State Ionics 135 (2000) 33.
[4] J.P. Maranchi, A.F. Hepp, P.N. Kumta, Electrochemistry and Solid State Letters 6 (2003) A198.
[5] C.K. Chan, H.L. Peng, G. Liu, K. Mcllwrath, X.F. Zhang, R.A. Huggins, Y. Cui, Nature Nanotechnology 3 (2008) 31.
[6] M.H. Park, M.G. Kim, J. Joo, K. Kim, J. Kim, S. Ahn, Y. Cui, J. Cho, Nano Letters 9 (2009) 3844.
[7] T. Song, J.L. Xia, J.H. Lee, D.H. Lee, M.S. Kwon, J.M. Choi, J. Wu, S.K. Doo, H. Chang, W. Il Park, D.S. Zang, H. Kim, Y.G. Huang, K.C. Hwang, J.A. Rogers, U. Paik, Nano Letters 10 (2010) 1710.
[8] H. Kim, M. Seo, M.H. Park, J. Cho, Angewandte Chemie International Edition 49 (2010) 2146.
[9] H. Kim, B. Han, J. Choo, J. Cho, Angewandte Chemie International Edition 47 (2008) 10151.
[10] S.H. Ng, J.Z. Wang, D. Wexler, K. Konstantinov, Z.P. Guo, H.K. Liu, Angewandte Chemie International Edition 45 (2006) 6896.
[11] J. Saint, M. Morcrette, D. Larcher, L. Laffont, S. Beattie, J.P. Peres, D. Talaga, M. Couzi, J.M. Tarascon, Advanced Functional Materials 17 (2007) 1765.
[12] X.S. Zhou, Y.X. Yin, L.J. Wan, Y.G. Guo, Chemical Communications 48 (2012) 2198.
[13] A. Magasinski, P. Dixon, B. Hertzberg, A. Kvit, J. Ayala, G. Yushin, Nature Materials 9 (2010) 353.
[14] L.F. Cui, Y. Yang, C.M. Hsu, Y. Cui, Nano Letters 9 (2009) 3370.
[15] A.A. Griffith, Philosophical Transactions of the Royal Society of London A 221 (1921) 163;
G. Irwin, Journal of Applied Mechanics 24 (1957) 361.
[16] J.C. Guo, Q. Liu, C.S. Wang, M.R. Zachariah, Advanced Functional Materials 22 (2012) 803.
[17] S.H. Ng, J. Wang, D. Wexler, S.Y. Chew, H.K. Liu, Journal of Physical Chemistry C 111 (2007) 11131.
[18] A.M. Wilson, B.M. Way, J.R. Dahn, T. Vanbuuren, Journal of Applied Physics 77 (1995) 2363.